Solution based approaches for the morphology control of $BaTiO_3$ particulates

Florentina Maxim[1], Paula Ferreira[1], Paula M. Vilarinho[1,*], Ian Reaney[2], Anne Aimable[3], Paul Bowen[3]

[1]*Electroceramics Group, Department of Ceramics and Glass Engineering, Centre for Research in Ceramics and Composites, CICECO, University of Aveiro, Portugal*
[2]*Department of Engineering Materials, University of Sheffield, Sheffield S1 3JD, United Kingdom*
[3]*Powder Technology Laboratory, Materials Department, Swiss Federal Institute of Technology Lausanne (EPFL), Switzerland*

Received 6 March 2010; received in revised form 18 September 2010; accepted 22 September 2010

Abstract

Within the action COST 539 - ELENA our contribution was aimed at studying solution based approaches for the morphology control of $BaTiO_3$ particulates. Initially, our kinetic analysis and systematic structural and morphological studies, demonstrated that during hydrothermal synthesis from layered titanate nanotubes (TiNTS), $BaTiO_3$ forms via two mechanisms depending on the temperature and time. At low temperatures (90°C), "wild" type $BaTiO_3$ dendritic particles with cubic structure were formed through a phase boundary topotactic reaction. At higher temperatures and/or for longer times time, the reaction is controlled by a dissolution precipitation mechanism and "seaweed" type $BaTiO_3$ dendrites are formed. Our results unambiguously elucidated why TiNTs do not routinely act as templates for the formation of 1D $BaTiO_3$.
In our subsequent investigations, the effect of additives on the aqueous and hydrothermal synthesis of $BaTiO_3$ was assessed. We reported that although the tested additives influenced the growth of $BaTiO_3$, their behaviour varied; poly(acrylic acid) (PAA) adsorbed on specific crystallographic faces changing the growth kinetics and inducing the oriented attachment of the particles; poly(vinyl pyrrolidone) (PVP), sodium dodecylsulfate (SDS) and hydroxypropylmethylcellulose (HPMC) act as growth inhibitors rather than crystal habit modifiers; and D-Fructose appeared to increase the activation energy for nucleation, resulting in small crystals (26 nm). Our work clearly indicates that the synthesis of 1D nanostructures of complex oxides by chemical methods is non trivial.

Keywords: *barium titanate, titanate nanotubes, anisotropic particles, hydrothermal synthesis, additive assisted synthesis*

I. Scaling of microelectronics

For applications as sensors, microactuators, infrared detectors, microwave phase filters and non-volatile memories, functional properties of ferroelectric materials such as switchable polarization, piezoelectricity, high non-linear optical activity, pyroelectricity, and non-linear dielectric behaviour are indispensable [1].

More recently and motivated by the industrial need of reduction of size of microelectronics devices to increase volumetric efficiency, many efforts have been dedicated to the development of new fabrication strategies of micro- and nano- scale ferroelectric structures. As dimensions decrease, ferroelectric materials exhibit a pronounced size effect, which is manifested in a significant deviation from bulk properties.

The interest in the fabrication of one-dimensional (1D) ferroelectric nanostructures such as nanowires (NWs) and nanotubes (NTs) has increased in the recent years for two important reasons. First, the study of these systems can provide useful information for the fabrication of next generation, fully three-dimensional FeRAM structures with the required bit density [2]. Second, de-

* Corresponding author: tel: +351 234 370354/259
fax: +351 234 370200, e-mail: *paula.vilarinho@ua.pt*

tailed *ab initio* calculations have predicted a new kind of ferroelectric order in nanorods and nanodisks [3,4].

II. Strategies for miniaturization

There are two main approaches for the preparation of 1D materials. The so called *top-down* methods that consist in the size reduction until 1D nano structures are obtained and *bottom-up* methods when atoms, ions or molecules are assembled [5].

The *top-down* methods based on electron-beam (EB) assisted fabrication involves patterning the ferroelectric structures either by milling of the ferroelectric layer using a focused ion beam (FIB) [6] or by maskless EB lithography [7]. Top-down methods are widely used in modern commercial nanotechnology because they provide high-precision positioning and size control. However, they are limited in resolution, time-consuming and are prone to processing damage [5].

Bottom-up methods include: use of the intrinsically anisotropic crystallographic structure of a solid to accomplish 1D growth; introduction of a liquid-solid interface to reduce the symmetry of a seed; use of various templates with 1D morphologies to direct the formation of 1D nanostructures; use of supersaturation control to modify the growth habit of a seed; use of appropriated capping reagents to kinetically control the growth rates of various facets of a seed; and self assembly of 0D nanostructures [8]. Among the *bottom-up* procedures, template assisted methods have been the most tried and tested for the preparation of 1D ferroelectric materials. In general, there are two main template based methods; denoted as 'physical' and 'chemical' templating. *Physical template* methods use templates with 1D morphologies in order to direct the growth of 1D product. After synthesis, the template must be removed either by thermal or chemical etching. *Chemical template methods* utilise 1D particles, which act as both template and precursor.

Physical template methods are based on filling porous templates with a solution containing the required precursors followed by thermal treatment to obtain a crystalline structure. By using electrophoresis for filling the pores of track-etched polycarbonate (PC), large areas of nanorods of $PbZr_xTi_{1-x}O_3$ (PZT) and $BaTiO_3$ ferroelectric materials have been grown [9]. Uniform nanorods (NRs) of 45–200 nm in diameter and 10 μm in length were grown over large areas with near unidirection alignment. The NRs had the desired stoichiometric composition and crystal structure after firing to 500–700°C up to one hour. Nanotubes (NTs) of $BaTiO_3$ and $PbTiO_3$ were prepared for the first time in 2002 by physical sol-gel template method [10]. Sol precursors were deposited by dip coating on anodized aluminium anodisc membranes and the template pores filled by capillarity. Later, Morrison *et al.* [11] reported an innovative method of filling the template pores by a liquid source 'mist' deposition technique. NTs of PZT, BT and $Sr_xBa_{1-x}TiO_3$ (SBT) with high aspect ratio, as large as 60 were grown on porous Si substrates.

Although physical template methods have the advantage of producing periodic arrays of 1D nanostructures, the main drawbacks are that the dimensions of the 1D structures are confined to the sizes of the template (usually larger in diameter than the required nanoparticle dimension) and the need of a post-deposition annealing process (often at high temperature).

To overcome these drawbacks *chemical template* methods using 1D nanostructures as both precursors and templates have been proposed. Although these methods are not straightforward and different mechanisms can nullify the template role of 1D precursors, smaller 1D ferroelectrics may be obtained at lower temperatures via these methods. Within this context the growth of titanate based ferroelectrics starting from TiO_2 NTs was studied. It was claimed that TiO_2 based nanotubes act as precursors for the hydrothermal preparation of $BaTiO_3$ 1D nanostructures [12]. However, at that time, the chemical nature of the nanotubes was not clearly identified and the obtained powders contained amorphous phases, unreacted titania nanotubes and carbonate impurities [13]. Later, Bao *et al.* reassessed this approach but the crystal structure of the NRs was not adequately proven [14]. Buscaglia *et al.* also reported the synthesis of single crystal $BaTiO_3$ nanowires with tetragonal structure by topochemical solid-state reaction at 700°C using layered TiO_2 nanowires as reactive templates coated with $BaCO_3$ nanocrystals [15]. According to the authors, the initial morphology of the titania nanowires was retained in the final product and the $BaTiO_3$ NWs exhibited strong piezoactivity and a striped domain structure.

Other bottom-up approaches used for the 1D nanostructure fabrication include additive assisted methods. It has been demonstrated that additives can be used as crystal growth modifiers by changing the growth habit or kinetically controlling the growth rate of various crystallographic facets [16,17]. Good examples of such additives are polymers, which can be adsorbed preferentially on specific crystallographic planes, thereby orienting the growth in a particular direction (the growth direction is determined by the slowest growing crystal face with the lowest surface energy) [18]. For instance, polyacrylic acid and polyethylene-oxide-block-polymethacrylic acid can adsorb specifically on {100}, and {110} crystallographic planes of barium titanate reducing their surface energy [19,20]. It is thus, expected that the growth direction of $BaTiO_3$ may be oriented in these directions. Although some morphological changes were observed by Bagwell *et al.* [20], no anisotropic growth was reported in this study and the barium titanate particles formed in the presence of the polymeric species were rounder than those formed without

any polymeric additives. In contrast, oriented growth of PZT single crystals was promoted by the specific adsorption of poly(vinyl alcohol) (PVA) and poly(acrylic acid) (PAA) on (001) crystallographic planes [16], resulting in the formation of PZT NWs. The large surface energy of the exposed (001) plane was reduced by the adsorption of PVA by hydrogen bonding. The energy reduction is further enhanced by the adsorption of PAA through carboxy group chemical bonding [16].

Using laurylamine as an additive, NRs of $BaTiO_3$ were prepared by a combined route based on sol-gel and surfactant templated methods at low temperature [17]. Isolated single-crystal, cubic perovskite $BaTiO_3$ nanorods with diameters ranging from 20 to 80 nm were formed by an oriented attachment mechanism [21]. The surfactant adsorbs on specific crystalline surfaces of the nanoparticles and modifies their growth direction. Therefore, the shape and size of particles in the system can be altered by oriented attachment of the primary nanoparticles. Depending on the orientation, further oriented attachment will result in the formation of rod-shaped structures [17].

III. Our contribution within COST 539

$BaTiO_3$ is one of the most widely used ferroelectric ceramic materials in passive electronic components, particularly in multilayer ceramics capacitors (MLCCs) [22]. In addition, there is currently renewed interest in $BaTiO_3$ with optimized piezoelectric performance as a possible lead free substitute for PZT [23]. Consequently, it was considered an ideal material upon which to base our activity within COST 539 ELENA. This paper therefore reports our contribution for a better understanding of the anisotropic growth of $BaTiO_3$ in aqueous solutions.

Two bottom-up approaches were used to determine the anisotropic growth of $BaTiO_3$ particles from solution. The first approach, a chemical templating method, used layered sodium titanate nanotubes (TiNTs) as precursors and $Ba(OH)_2$ as the aqueous media. It was unambiguously demonstrated by kinetic studies that two nucleation and growth mechanisms take place depending on the synthesis temperature and time. In the second approach, additives were used as crystal modifiers to control the growth of $BaTiO_3$ in aqueous and hydrothermal syntheses [24,25].

The kinetic analysis in the first approach was based on the Johnson-Mehl-Avrami (JMA) model, generally used to determine the crystallization in solid state reactions [26,27]. It has also previously been applied to the formation of round shaped particles of $BaTiO_3$ under hydrothermal conditions [28–30]. This model postulates that for reactions obeying a single theoretical rate equation plots of $\ln[-\ln(1-f)]$ versus $\ln(t)$, where f is the fraction of crystallization at time t, over the range $f = 0.15–0.50$ yield approximately straight lines, with

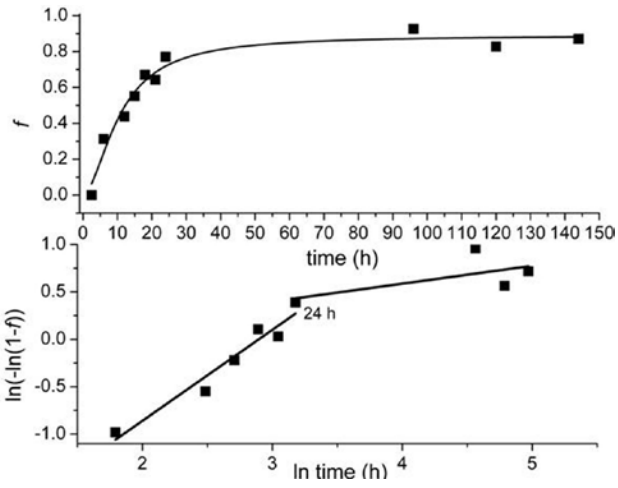

Figure 1. a) The $BaTiO_3$ crystalline fraction (f) as a function of the synthesis time, t for the samples prepared by hydrothermal treatment starting from TiNTs at 110°C and b) the corresponding Johnson-Mehl Avrami plot

slope (m) characteristic of three distinct reaction mechanisms [31]; for $m = 0.54–0.62$, diffusion is the rate limiting step, for $m = 1.0–1.24$, a zero-order, first-order, or a phase-boundary controlled mechanism is indicated and, when $m = 2.0–3.0$, the nucleation controls the rate.

In our studies, the variation of crystallized $BaTiO_3$ fraction with time (Fig. 1a) and the JMA plots (Fig. 1b) indicated that crystallization of $BaTiO_3$ takes place in two stages, in a similar manner to that previously reported [28–30]. A value of $m \approx 1$ was obtained in the first regime and corresponds to a phase boundary mechanism [31] in agreement with Walton *et al.* [32] in which $BaTiO_3$ was synthesized in a static hydrothermal cell from an amorphous TiO_2 precursor and $Ba(OH)_2$ aqueous media. For the synthesis of $BaTiO_3$ via aqueous co-precipitation or in non-static hydrothermal cells [28–30] values as high as $m = 2.63$ have been reported and attributed to nucleation dominated mechanisms. Our data therefore indicate a fundamentally different rate-determining step in static hydrothermal synthesis of $BaTiO_3$ starting from TiNTs compared to other methods. For the second regime, a value of $m \approx 0.2$ was obtained independent on the synthesis temperature. According to the JMA model this value does not fall into any of the three listed exponent ranges [31]. However, the JMA model is only valid for $f \leq 0.5$ and in the second stage the fraction of $BaTiO_3$ crystallization is > 0.7. Therefore, a detailed structural and morphological study was performed to understand further the crystallization process.

In agreement with the exponent $m \approx 1$ or $f < 0.7$, TEM studies clearly demonstrate that $BaTiO_3$ nucleates on the surface of the TiNTs (Fig. 2). It was postulated that when the TiNTs start to dissolve a sequence of reactions to form hydrous titanium cations ($Ti(OH)_x^{(4-x)+}$) takes place. At each hydrolysis step however, H_3O^+ ions are generated [33]. Under the current static synthesis

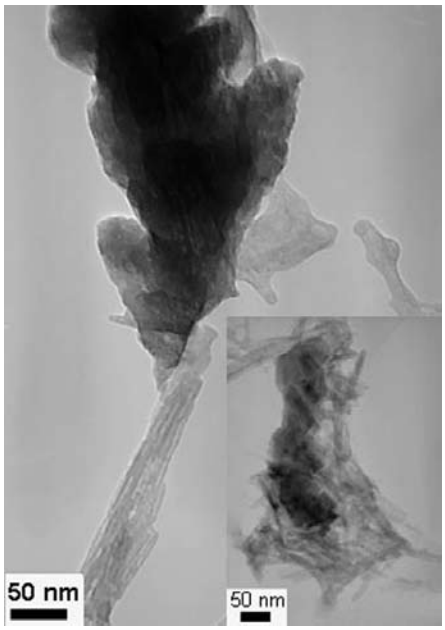

Figure 2. TEM micrograph of a sample prepared at the early stages of the reaction at 110°C illustrating the nucleation of $BaTiO_3$ on the TiNTs surface. In the inset a similar sample prepared at 200°C

conditions, the local concentration of Ti at the surface of the NTs increases and therefore local pH decreases. The decrease in local pH shifts the equilibrium of the hydrolysis reactions to the left, thereby suppressing the formation of $Ti(OH)_4$ which is critical for the formation of $BaTiO_3$ [33]. The proposed rate-determining step (RDS) therefore relates.

not to nucleation or diffusion but to the hydrolysis of the Ti precursor at the surface of the titanate NTs. This RDS corresponds directly to the phase boundary mechanism indicated by the exponent, m ≈ 1 obtained from fitting of the kinetic data.

The structural analysis suggested also that there is a gradual transition from pseudocubic to tetragonal barium titanate with the reaction temperature and time. This is indicated by the reflections around 2θ of 45° [(200) and (002)] in the X-Ray patterns which became broader as the temperature and time of reaction increases (see Fig. 3). The splitting of the reflection at $2\theta \approx 45°$ is characteristic of the tetragonal distortion of the $BaTiO_3$ structure. This cell distortion is reflected also in the Raman spectra [24,25] by the appearance of the sharp band at ~ 307 cm^{-1} [34]. We postulate therefore, that at the early stages of $BaTiO_3$ crystallization cubic $BaTiO_3$ is more likely to form whereas at later stages predominately tetragonal $BaTiO_3$ particles are obtained [24,25].

The stabilization of *pseudo* cubic structure of $BaTiO_3$ is commonly reported for hydrothermal synthesis [35–37]. It has been suggested that the reason for this behaviour is the presence of lattice defects created by replacing the O^{2-} ions on the oxygen sublattice with OH^-. The most likely compensation mechanism(s) for substitution of O^{2-} by OH^- is by the formation of cation vacancies, although the precise defect chemistry remains controversial. The presence of cation vacancies is accompanied by local distortions of the lattice which suppress long range cooperative tetragonal distortion and a pseudocubic phase is obtained.

In SEM micrographs, we observed that the transition from pseudocubic to tetragonal is accompanied by a change in the particle morphology from "wild"-type dendrites to round shaped particles and "seaweed" dendrites (Fig. 4). At low synthesis temperature (90°C) and short reaction times "wild" type dendrites with a rough defective surface are formed (Fig. 4a). As the crystallised $BaTiO_3$ fraction increases with the temperature and time, round shaped particles are observed (Fig. 4b) followed by defect free dendritic particles with smooth surface called "seaweed" type (Fig. 4c).

In the present study we have demonstrated that a topotactic reaction takes place at the TiNTs surface, which resulted in the nucleation of $BaTiO_3$ at the nanotube surface. A topotactic reaction is essential if 1D $BaTiO_3$ nanostructures are to be attained. However, our observations contradict those reported by Mao *et al.* [12] and

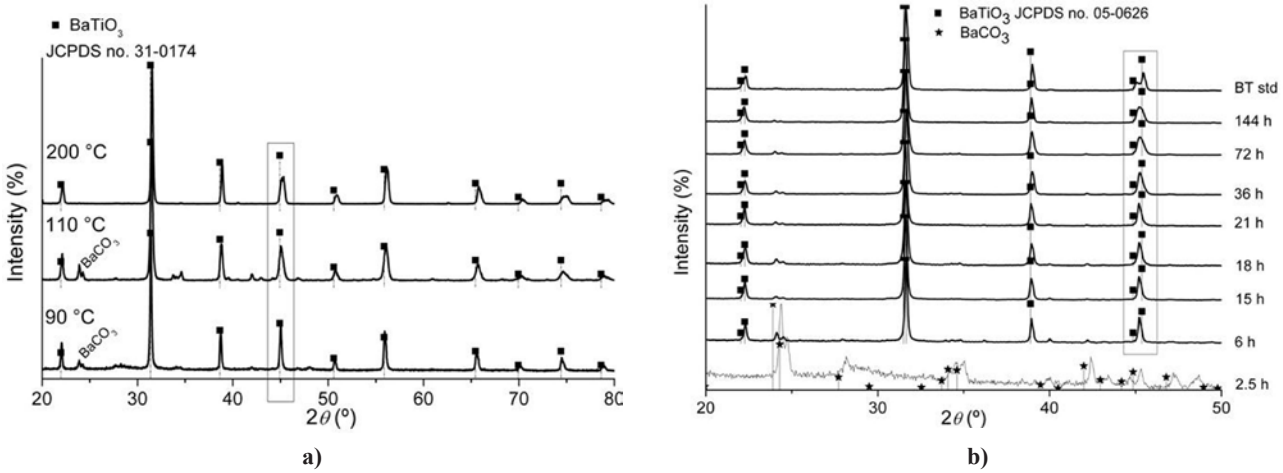

a) **b)**

Figure 3. X-Ray diffraction patterns for the samples prepared by hydrothermal treatment starting from TiNTs illustrating the influence of a) synthesis temperature and b) synthesis time

Bao *et al.* [14] who claimed that the nanotubular morphology of the titanium precursor can be preserved during the in-situ topotactic reaction at low temperatures and times of hydrothermal synthesis, with the formation of NTs and NRs of $BaTiO_3$, respectively. Instead, dendritic growth was observed which effectively overwrote the nanotubular morphology of the precursor. This implies that the use of layered titanate nanotubes as templates to prepare $BaTiO_3$ nanorods/nanotubes is challenging.

In the <u>*second approach*</u> we used various additives in the aqueous and hydrothermal synthesis of $BaTiO_3$ starting from $Ba(OH)_2$ and titanium butoxide as the barium and titanium sources, respectively. It should be noted in the aqueous and hydrothermal syntheses, starting from alkoxides, the formation of $BaTiO_3$ takes place in two steps [38]. In the first step Ti-O-Ti network is rapidly formed by hydrolysis-condensation of the titanium alkoxide with the formation of amorphous titanium hydroxide. The second step consists in the slow reaction of Ba ions with amorphous titanium hydroxide to form $BaTiO_3$ [38]. Once a nucleus is formed the crystal shape will depend on the kinetic growth factors, which can be drastically modified by the presence of crystal habit modifiers, which preferentially adsorb on a specific crystal face [18]. Within this context, we systematically studied the effect on the synthesis of $BaTiO_3$ of three different categories of crystal habit modifiers; i) polymers, poly(acrylic acid) (PAA) and poly(vinyl pyrrolidone) (PVP); ii) a surfactant, sodium dodecylsulfate (SDS); and iii) the carbohydrates, hydroxypropylmethylcellulose (HPMC) and (D-)fructose with a view to obtaining 1D $BaTiO_3$ nanoparticles.

Syntheses was separated into two steps in order optimize crystallinity. First, a pre-treatment of the precursors mixtures at 96°C was performed, followed by a hydrothermal treatment at 110°C. X-Ray diffraction revealed that, crystalline barium titanate was obtained in the pre treatment step before hydrothermal treatment in the presence of PAA, PVP, SDS and HPMC irrespective of the additive concentration (0.4 g/l for the low concentration and 5 g/l for the high concentration). The only exception was in the case of a high concentration of fructose when no $BaTiO_3$ was formed before hydrothermal treatment. Fig. 5 present the X-ray patterns of the samples obtained after the hydrothermal treatment for low and high additive concentrations, respectively. $BaTiO_3$ with low crystallinity is formed in the presence of high concentrations of D-fructose (Fig. 5b).

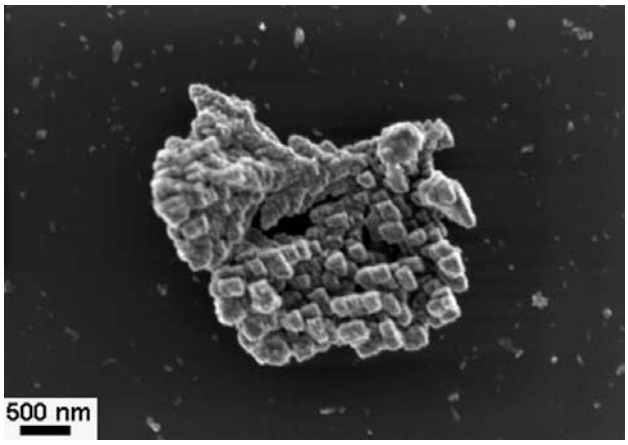

a)

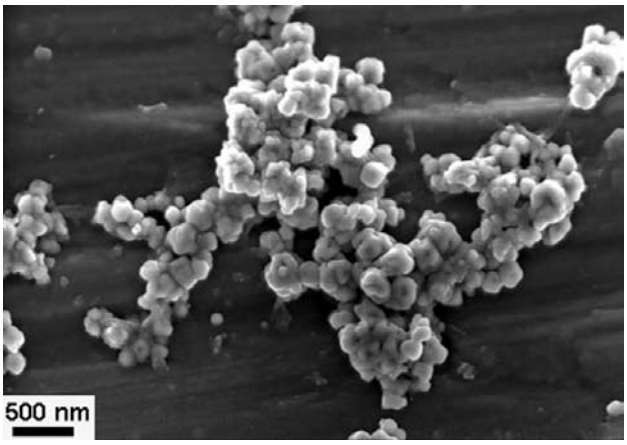

b)

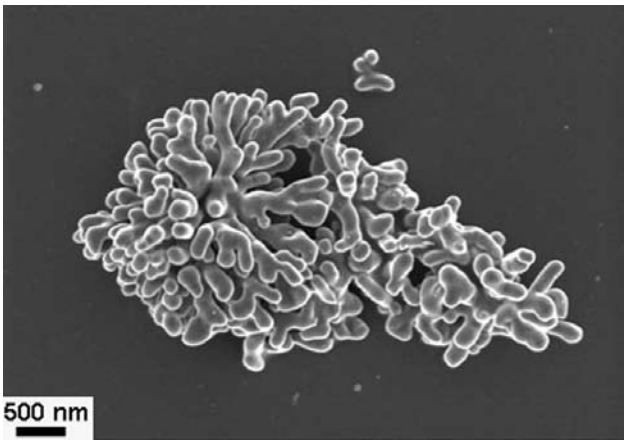

c)

Figure 4. SEM micrographs of a) "wild"-type dendrites b) round shaped particles and c) "seaweed" dendrites showing the morphological evolution when increasing the synthesis temperature and time

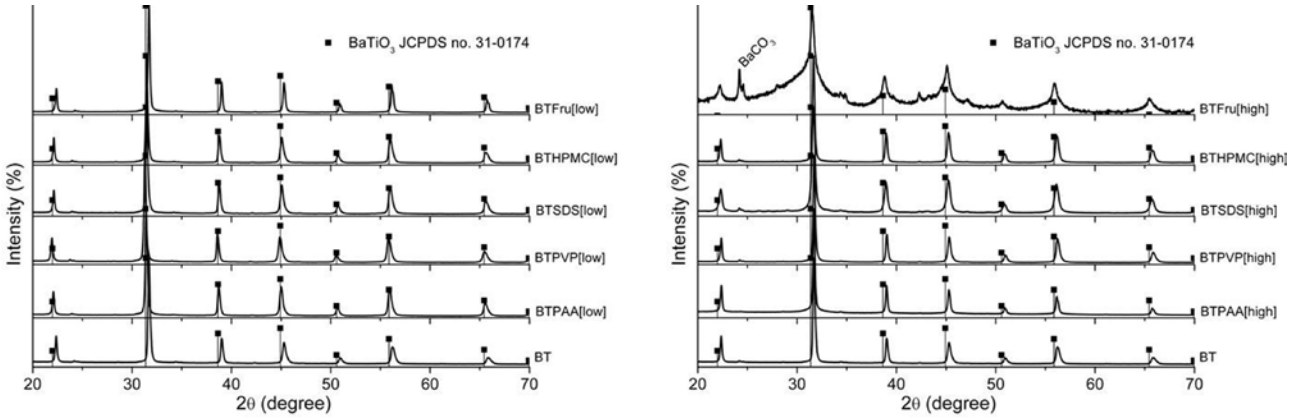

Figure 5. X-ray diffraction patterns of the samples prepared after the hydrothermal synthesis in the presence of the additives (PAA, PVP, SDS, HPMC and Fructose) for a) low and b) high concentration

Table 1. The specific surface areas (S_{BET}), the equivalent spherical particle diameters (d_{BET}), the crystallite size (d_{XRD}) and the factor of aggregation of the samples obtained in this study

Pre-treatment step					*Hydrothermal treatment*				
Sample index	S_{BET} [m²/g]	d_{BET} [nm]	d_{XRD} [nm]	F_{agg}	Sample index	S_{BET} [m²/g]	d_{BET} [nm]	d_{XRD} [nm]	F_{agg}
BTpp	13.5	74	70	3	BT	11.2	89	42	3
BTpp-PAA[low]	18.6	54	61	22	BT-PAA[low]	13.0	77	42	3
BTpp-PAA[high]	18.5	54	58	21	BT-PAA[high]	16.0	62	66	11
BTpp-PVP[low]	16.4	61	63	31	BT-PVP[low]	12.8	78	39	29
BTpp-PVP[high]	16.4	61	34	4	BT-PVP[high]	12.5	80	47	9
BTpp-SDS[low]	14.9	67	33	13	BT-SDS[low]	13.3	75	42	3
BTpp-SDS[high]	54.7	18	22	207	BT-SDS[high]	30.8	32	25	29
BTpp-HPMC[low]	19.2	52	65	46	BT-HPMC[low]	10.4	96	43	16
BTpp-HPMC[high]	30.5	33	26	69	BT-HPMC[high]	13.1	76	43	5
BTpp-Fru[low]	21.0	47	59	39	BT-Fru[low]	15.4	65	75	4
BTpp-Fru[high]	160.0	N/A	N/A	N/A	BT-Fru[high]	179.3	N/A	N/A	N/A

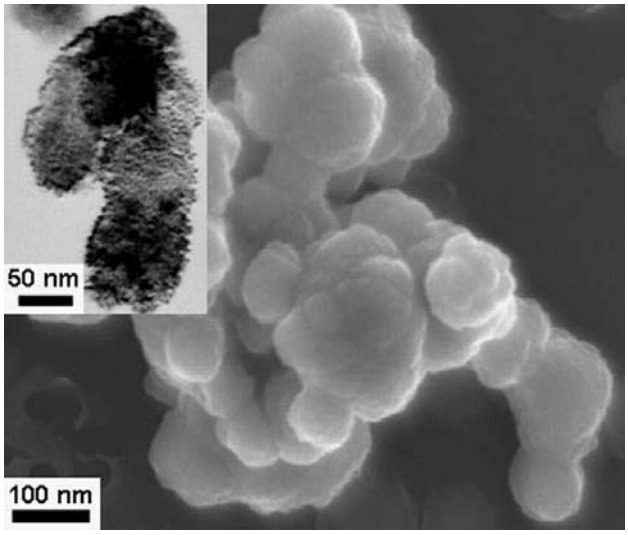

Figure 6. Microstructure (by SEM) of the sample prepared in the presence PAA at high concentration illustrating the oriented attachment and porous feature of $BaTiO_3$ particles

In the case of a high concentration of PAA, direct aggregation of $BaTiO_3$ particles was promoted (Fig. 6). Similar specific surface areas (S_{BET}) were obtained independent of the additive concentration (Table 1) and high weight loss was observed at higher PAA concentrations (Table 2). PAA adsorption at high pH occurs through hydrogen bonding or some specific bonding of the polymer to ion sites at the surface [20]. At high pH (in this case pH > 12), PAA is fully ionized, with free COO^- groups. At pH > 10 the barium titanate particles have negative surface charge [39]. Therefore, the most probable adsorption mechanism of PAA on the barium titanate surface is by specific bonding to the $BaTiO_3$ particle surface by Ba bridges [40]. This situation is favoured by the formation of a monodentate, Ba-PAA complex (Ba^+-COO). If the Ba^{2+} ions form a bidentate species no positive charge remains to bind the polymer with the barium titanate surface sites. As a result, the polymer is trapped during the precipitation rather than adsorbed onto the particle surface.

Table 2. The weight loss calculated from TGA curves of the samples obtained in this study

Sample	Mass Loss [%]			Sample	Mass Loss [%]		
	< 200°C	200–600°C	600–800°C		30–200°C	200–600°C	600–800°C
BTpp	0.3	2.4	0.2	BT	0.1	1.8	0.1
BTpp-PAA[low]	0.3	2.8	0.3	BT-PAA[low]	0.1	2.3	0.2
BTpp-PAA[high]	0.9	5.8	1.8	BT-PAA[high]	0.5	6.0	0.8
BTpp-Fru[low]	0.6	2.3	0.3	BT-Fru[low]	0.2	2.8	0.3
BTpp-Fru[high]	2.1	5.9	1.0	BT-Fru[high]	1.3	6.5	0.7
BTpp-PVP[low]	0.3	2.5	0.3	BT-PVP[low]	0.1	1.8	0.2
BTpp-PVP[high]	0.3	2.6	0.2	BT-PVP[high]	0.1	2.4	0.2
BTpp-SDS[low]	0.4	2.5	0.2	BT-SDS[low]	0.1	2.0	0.1
BTpp-SDS[high]	0.8	4.8	0.4	BT-SDS[high]	0.6	4.2	0.4
BTpp-HPMC[low]	0.3	2.8	0.2	BT-HPMC[low]	0.1	2.0	0.1
BTpp-HPMC[high]	0.5	6.3	0.2	BT-HPMC[high]	0.2	5.9	0.2

Pores within $BaTiO_3$ particles prepared in the presence of PAA are revealed by TEM (see inset of Fig. 6). The similar value of S_{BET} irrespective of the additive concentration supports the notion that PAA is trapped during the $BaTiO_3$ precipitation rather than adsorbed on the particle surface. Therefore, we can state that PAA controls the $BaTiO_3$ nucleation under the applied experimental conditions. PAA also influences the growth of $BaTiO_3$ as indicated by direct aggregation (Fig. 6), suggesting that the growth is controlled by a mechanism often referred to as oriented attachment [41]. A similar mechanism has been reported for when two adjacent anatase nanoparticles come into the same crystallographic orientation. High-energy faces fuse and the result is an aggregate with directed orientation [42]. In our case, it is possible that PAA preferentially adsorbs on high energy $BaTiO_3$ crystallographic faces, decreasing the growth rate of these faces and inducing oriented attachment of the $BaTiO_3$ particles. Thus, we can state that PAA limits the growth kinetics of $BaTiO_3$ by decreasing the surface energy and thereby decreasing the growth rates of specific crystallographic faces.

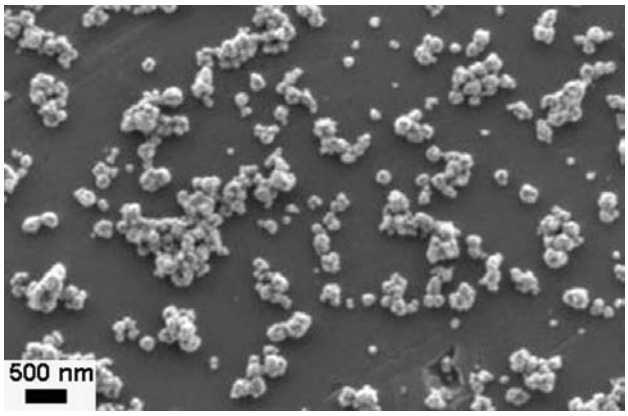

Figure 7. Microstructure (by SEM) of the sample prepared in the presence PVP at high concentration illustrating disperse and homogeneous $BaTiO_3$ particles

PVP is a water soluble polymer with a basic character which may strongly interact with other molecules by the formation of hydrogen bonds that act as proton acceptors [43]. Because of these properties, PVP can be coordinately bonded to the surface ions and forms a protective layer, which impedes further aggregation, thereby acting as a growth inhibitor and dispersant [44]. Our studies revealed that the morphology of the barium titanate particles is not changed in the presence of PVP since we obtained round particles (80–100 nm) similar to blank samples. However, because better dispersed and homogeneous particles are formed (Fig. 7), it is suggested that the colloidal stability was increased by a steric effect in the presence of PVP. The steric repulsion effect on the $BaTiO_3$ nuclei may be related to the high viscosity of PVP in aqueous solution [45], which reduces the mobility of the nucleus and consequently the agglomeration. The roll of this additive as a growth inhibitor is indicated by the reduction of the crystallite size (Table 1) from 70 nm (in the blank) to 34 nm (for high PVP concentration). As the weight loss of the samples prepared in the presence of PVP is independent of concentration (Table 2), we consider that this additive is not adsorbed onto the $BaTiO_3$ surface. Taking into account all the above data, we propose that PVP is influencing the growth of $BaTiO_3$ but does not act as a crystal habit modifier.

SDS is an anionic surfactant with critical micelle concentration of 0.252 g / 100 cm^3 at 30°C [46]. In general, surfactants can influence the growth in two ways: i) by creating direct micelles (oil in water) the surfactant acts as a growth inhibitor [47] and ii) as a capping molecule, they can adsorb on specific crystallographic faces, influence the growth kinetics, and modify crystal shape [17]. In the present study SDS acted as growth inhibitor rather than as a crystal modifier since the crystallite size was drastically reduced (Table 1) and no changes in the particle shape was observed. However, the colloidal stability was reduced

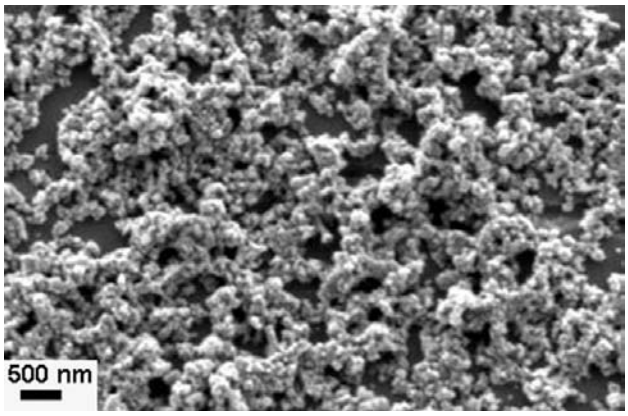

Figure 8. Microstructure (by SEM) of the sample prepared in the presence SDS at high concentration illustrating the high degree of agglomeration

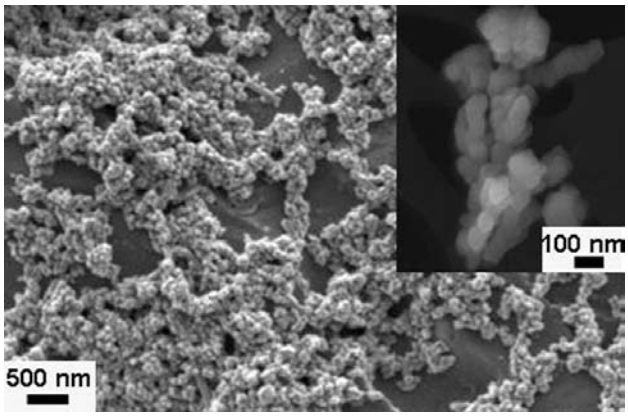

Figure 9. Microstructure (by SEM) of the sample prepared in the presence HPMC at high concentration illustrating the various $BaTiO_3$ particles morphologies

when using SDS and more agglomerated powders were obtained (Fig. 8 and Table 1).

The HPMC is a polysaccharide derived from cellulose by insertion of hydrophobic moieties such as hydroxypropyl and methyl. HPMC presents a high hydrophilic character due to the presence of polyhydroxy groups on the molecular chains, which make the polymer water soluble [48]. Due to the presence of both hydrophilic and hydrophobic groups, HPMC presents unique hydration-dehydration properties and can act as crystal modifier by creating bonds with either hydrophobic or hydrophilic crystal faces. The role of crystal modifier of HPMC has been verified in the case of the crystal growth of copper oxalate [49] and $CaCO_3$ [50] when the HPMC selectively interacts with the hydrophobic faces of the crystal, restricting the crystal growth in one direction. Another important characteristic of HPMC is its inverse solubility and gelation, i.e., HPMC becomes less soluble in water when the temperature increases and eventually becomes a hydrogel with a 3D network [51]. HPMC can act as growth inhibitor since the crystal growth can be regulated and restricted by the 3D network structure of HPMC gel. In the present study, we observed the formation of particles with various morphologies when increasing the HPMC concentration (Fig. 9). Small agglomerated particles with rough surface, dendritic particles with a smooth surface and particles with parallelepiped shape were obtained. Energy dispersive X-ray mapping confirmed that Ti and Ba are homogeneously distributed in all the observed morphologies, indicating that various stages of $BaTiO_3$ crystallization can be observed at this reaction level. When the HPMC is in solution, round shape particles are formed but when the HPMC gel is formed by increasing the reaction temperature and concentration, the crystal growth of $BaTiO_3$ will be inhibit and modulated and anisotropic barium titanate particles can be obtained. The roll of HPMC as a growth inhibitor is confirmed by the variation of crystallite size from 70 nm in the blank sample to 26 nm at high HPMC concentration (Table 1). Moreover, the value of S_{BET} is twice as high as in the blank for large HPMC concentrations (Table 1) which suggests the presence of amorphous phase, often formed in incomplete sol-gel reactions [52]. This result is an indication of delayed $BaTiO_3$ crystallization when the

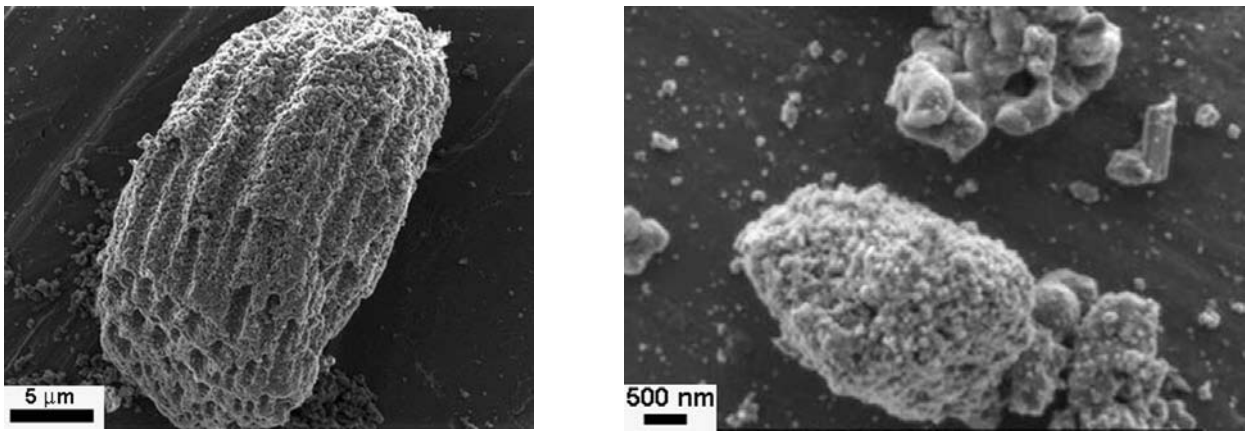

a) **b)**

Figure 10. Microstructure (by SEM) of the sample prepared in the presence Fructose at high concentration illustrating the formation of large agglomerates of equiaxed particles; a) before and b) after the hydrothermal treatment

concentration of HPMC is increased, as in the case of $CaCO_3$ crystallization [50]. Based on the obtained results we can state that HPMC acts mainly in the present conditions as a growth inhibitor of $BaTiO_3$.

From our studies, the most evident effect of additive concentration on the $BaTiO_3$ crystallization was observed in the case of D-Fructose. At low concentration, round shaped $BaTiO_3$ particles, similar to the blank sample, were formed but at high additive concentration large agglomerates of equiaxed particles, which seems to be organized into an ordered porous structure, were formed (Fig. 10a). However, no peaks associated with $BaTiO_3$ were identified by XRD analysis. $BaTiO_3$ with low crystallinity was formed only after the hydrothermal synthesis at 110°C (Fig. 5b) when the porous structure collapse and large agglomerates of particles formed (Fig. 10b). It is evident then, that the energy barrier for barium titanate nucleation is increased as the additive concentration increases. Similar behaviour has been observed in the case of $CaCO_3$ crystallization in the presence of saccharides [53]. This behaviour is probably an expression of Ostwald's step rule which stipulates that the nucleation rate of a metastable phase can be higher than those of the stable phases due to the local decrease of the supersaturation [54]. However, how saccharides, in general, and fructose, in particular affect crystallization remains to be elucidated. We believe that in the particular case of $BaTiO_3$ the local decrease of supersaturation can be due to the formation of stable Ba-fructose complexes, which restrict the reaction with the titanium precursor, and consequently the crystallization of $BaTiO_3$.

IV. Conclusions

i) Our work demonstrates that, for the formation of $BaTiO_3$ by chemical template hydrothermal synthesis starting from layered titanate nanotubes, two mechanisms take place depending on the temperature and time [24,25]. At low temperature and low time 'wild' type dendritic particles with pseudo-cubic structure have been formed by a phase boundary topotactic reaction on the TiNTs surface. At intermediate temperature and time round shaped particles of $BaTiO_3$ were formed. Finally, at high temperature and longer time 'seaweed' type dendrites with predominately tetragonal structure were obtained. In the last case the $BaTiO_3$ crystallization process was controlled by a dissolution-precipitation mechanism. Our work clearly shows that TiNTs can not easily act as directing growth agents or as template for hydrothermal synthesis of 1D $BaTiO_3$. Although at low temperature and low time topotactic reactions on the NTs surface takes place, their instability in the high alkaline solution results in a dissolution rate faster than that of $BaTiO_3$ nucleation.

ii) Our results give useful insights on how additives control barium titanate growth from aqueous solutions. PAA can adsorb on specific crystallographic $BaTiO_3$ faces changing the growth kinetics and inducing oriented attachment of the particles. PVP acts as a growth inhibitor rather than crystal habit modifier and small, well dispersed $BaTiO_3$ crystals are obtained. Due to micelle formation, SDS inhibits growth and $BaTiO_3$ with a crystallite size (26 nm) is formed. HPMC also acts as growth inhibitor due to its inverse water solubility and formation of viscous hydrogel. D-Fructose has the most evident effect on the $BaTiO_3$ crystallization and presents a threshold concentration for $BaTiO_3$ nucleation.

iii) The synthesis of 1D nanostructures of complex oxide by chemical methods is not a trivial task and more systematic studies on the synthesis and rigorous sample characterization are critically needed.

Acknowledgements: The authors acknowledge the Portuguese Foundation for Science and Technology (FCT), FEDER, the European Network of Excellence FAME, under the Contract FP6-500159-1 and COST 539, Electroceramics from Nanopowders Produced by Innovative Methods (ELENA). Florentina Maxim is thankful to FCT for the fellowship SFRH/BD/23375/2005.

References

1. J.F. Scott, C.A. Araujo, "Ferroelectric memories", *Science*, **246** (1989) 1400–1405.
2. J.F. Scott, F.D. Morrison, M. Miyake, P. Zubko, X.J. Lou, V.M. Kugler, S. Rios, M. Zhang, T. Tatsuta, O. Tsuji, T.J. Leedham, "Recent materials characterizations of [2D] and [3D] thin film ferroelectric structures", *J. Am. Ceram. Soc.*, **8** [7] (2005) 1691–1701.
3. A.N. Morozovska, E.A. Eliseev, M.D. Glinchuk, "Size effects and depolarization field influence on the phase diagrams of cylindrical ferroelectric nanoparticles", *Physica B*, **387** (2007) 358–366.
4. I.I. Naumov, L. Bellaiche, H. Fu, "Unusual phase transitions in ferroelectric nanodisks and nanorods", *Nature*, **432** (2004) 737–740.
5. A. Gruverman, A. Kholkin, "Nanoscale ferroelectrics: processing, characterization and future trends", *Reports Progress Phys.*, **69** (2006) 2443–2474.
6. A. Stanishevsky, S. Aggarwal, A.S. Prakash, J. Melgailis, R. Ramesh, "Focused ion-beam patterning of nanoscale ferroelectric capacitors", *J. Vac. Sci. Technol. B*, **16** (1998) 3899–3902.
7. M. Alexe, C. Harnagea, D. Hesse, U. Gosele, "Patterning and switching of nanosize ferroelectric memory cells", *Appl. Phys. Lett.*, **75** (1999) 1793–1795.
8. Y. Xia, P. Yang, Y. Sun, Y. Wu, B. Mayers, B. Gates, Y. Yin, F. Kim, H. Yan, "One -dimensional nanostructures: Synthesis, characterization, and applications", *Adv. Mater.*, **15** [5] (2003) 353–389.
9. S.J. Limmer, S. Seraji, M.J. Forbess, Y. Wu, T.P. Chou, C. Nguyen, G.Z. Cao, "Electrophoretic growth of lead zirconate titanate nanorods", *Adv. Mater.*, **13** [16] (2001) 1269–1272.

10. B.A. Hernandez, K-S. Chang, R.E. Fisher, P.K. Dorhout, "Sol-gel template synthesis and characterization of $BaTiO_3$ and $PbTiO_3$ nanotubes", *Chem. Mater.*, **14** (2002) 480–482.
11. F.D. Morrison, Y. Luo, I. Szafraniak, V. Nagarajan, R.B. Wehrspohn, M. Steinhart, J.H. Wendorff, N.D. Zakharov, E.D. Mishina, K.A. Vorotilov, A.S. Sigov, S. Nabayashi, M. Alexe, R. Ramesh, J.F. Scott, "Ferroelectric nanotubes", *Rev. Adv. Mater. Sci.*, **4** (2003) 114–122.
12. Y. Mao, S. Banerjee, S.S. Wong, "Hydrothermal synthesis of perovskite nanotubes", *Chem. Commun.*, **3** (2003) 408–409.
13. Y. Mao, T-J. Park, F. Zhang, H. Zhou, S.S. Wong, "Environmentally friendly methodologies of nanostructure synthesis", *Small*, **3** [7] (2007) 1122–1139.
14. N.Z. Bao, L.M. Shen, G. Srinivasan, K. Yanagisawa, A. Gupta, "Shape-controlled monocrystalline ferroelectric barium titanate nanostructures: From nanotubes and nanowires to ordered nanostructures", *J. Phys. Chem. C*, **112** [23] (2008) 8634–8642.
15. M.T. Buscaglia, C. Harnagea, M. Dappiagi, V. Buscaglia, A. Pignolet, P. Nanni, "Ferroelectric $BaTiO_3$ nanowires by a topochemical solid-state reaction", *Chem. Mater.*, **21** [21] (2009) 5058–5065.
16. G. Xu, Z.H. Ren, P.Y. Du, W.J. Weng, G. Shen, G.R. Han, "Polymer-assisted hydrothermal synthesis of single-crystalline tetragonal perovskite $PbZr_{0.52}Ti_{0.48}O_3$ nanowires", *Adv. Mater.*, **17** [7] (2005) 907–910.
17. S.Y. Zhang, F.S. Jiang, G. Qu, C.Y. Lin, "Synthesis of single-crystalline perovskite barium titanate nanorods by a combined route based on sol-gel and surfactant-templated methods", *Mater. Lett.*, **62** [16] (2008) 2225–2228.
18. J.A. Dirksen, T.A. Ring, "Fundamentals of crystallization: kinetic effects on particle size distributions and morphology", *Chem. Eng. Sci.*, **46** [10] (1991) 2389–2427.
19. A. Gruverman, O. Auciello, H. Tokumoto, ,"Imagin and control of domain structures in ferroelectric thin films via scanning force microscopy", *Annu. Rev. Mater. Sci.*, **28** (1998) 101–123.
20. R.B. Bagwell, J. Sindel, W. Sigmund, "Morphological evolution of barium titanate synthesized in water in the presence of polymeric species", *J. Mater. Res.*, **14** [5] (1999) 1844–1851.
21. L.R. Penn, J.F. Banfield, "Imperfect oriented attachment: Dislocation generation in defect-free nanocrystals", *Science*, **281** (1998) 969–971.
22. D. Hennings, M. Klee, R. Waser, "Advanced dielectrics - Bulk ceramics and thin-films", *Adv. Mater.*, **3** [7-8] (1991) 334–340.
23. S. Shao, J. Zhang, Z. Zhang, P. Zheng, M. Zhao, J. Li, C. Wang, "High piezoelectric properties and domain configuration in $BaTiO_3$ ceramics obtained through the solid-state reaction route", *J. Phys. D: Appl. Phys.*, **41** (2008) Art. No. 125408.
24. F. Maxim, P. Ferreira, P.M. Vilarinho, I. Reaney, "Hydrothermal synthesis and crystal growth studies of $BaTiO_3$ using Ti nanotube precursors", *Cryst. Growth Des.*, **8** [9] (2008) 3309–3315.
25. F. Maxim, P.M. Vilarinho, P. Ferreira, I. Reaney, I. Levin, "Kinetic study of the static hydrothermal synthesis of $BaTiO_3$ using titanate nanotubes precursors", *Chem. Mater.*, submitted, 2010.
26. M. Avrami, "Kinetics of phase change I - General theory", *J. Chem. Phys.*, **7** [12] (1939) 1103–1112.
27. M. Avrami, "Granulation, phase change, and microstructure - Kinetics of phase change. III", *J. Chem. Phys.*, **9** [2] (1941) 177–184.
28. J.O. Eckert Jr., C.C. Hung-Houston, B.L. Gersten, M.M. Lencka, R.E. Riman, "Kinetics and mechanisms of hydrothermal synthesis of barium titanate", *J. Am. Ceram. Soc.*, **79** [11] (1996) 2929–2939.
29. M. Viviani, M.T. Buscaglia, A. Testino, V. Buscaglia, P. Bowen, P. Nanni, "The influence of concentration on the formation of $BaTiO_3$ by directreaction of $TiCl_4$ with $Ba(OH)_2$ in aqueous solution", *J. Eur. Ceram. Soc.*, **23** (2003) 1383–1390.
30. J. Moon, E. Suvaci, A. Morrone, S.A. Costantino, J.H. Adair, "Formation mechanisms and morphological changes during the hydrothermal synthesis of $BaTiO_3$ particles from a chemically modified, amorphous titanium (hydrous) oxide precursor", *J. Eur. Ceram. Soc.*, **23** [12] (2003) 2153–2161.
31. J.D. Hancock, J.H. Sharp, "Method of comparing solid-state kinetic data and its application to decomposition of kaolinite, brucite, and $BaCO_3$", *J. Am. Ceram. Soc.*, **55** [2] (1972) 74–77.
32. R.I. Walton, F. Millange, R.I. Smith, T.C. Hansen, D. O'Hare, "Real time observation of the hydrothermal crystallization of barium titanate using in situ neutron powder diffraction", *J. Am. Chem. Soc.*, **123** (2001) 12547–12555.
33. M.M. Lencka, R.E. Riman, "Thermodynamic modeling of hydrothermal synthesis of ceramic powders", *Chem. Mater.*, **5** [1] (1993) 61–70.
34. Y. Shiratori, C. Pithan, J. Dornseiffer, R. Waser, "Raman scattering studies on nanocrystalline $BaTiO_3$ - Part I - isolated particles and aggregates", *J. Raman Spectroscopy*, **38** [10] (2007) 1288–1299.
35. H.J. Chen, Y.W. Chen, "Hydrothermal synthesis of barium titanate", *Indust. Eng. Chem. Res.*, **42** [3] (2003) 473–483.
36. D.F.K. Hennings, C. Metzmacher, B.S. Schreinemacher, "Defect chemistry and microstructure of hydrothermal barium titanate", *J. Am. Ceram. Soc.*, **84** [1] (2001) 179–182.
37. R. Vivekanandan, T.R.N. Kutty, "Characterization of barium titanate fine powders formed from hydrothermal crystallization", *Powder Technol.*, **57** [3] (1989) 181–192.
38. A. Testino, V. Buscaglia, M.T. Buscaglia, M. Viviani, P. Nanni, "Kinetic modeling of aqueous and hydrothermal synthesis of barium titanate ($BaTiO_3$)", *Chem. Mater.*, **17** (2005) 5346–5356.

39. Z.C. Chen, T.A. Ring, J. Lemaitre, "Stabilization and processing of aqueous $BaTiO_3$ suspension with polyacrylic-acid", *J. Am. Ceram. Soc.*, **75** [12] (1992) 3201–3208.
40. I. Pochard, P. Couchot, A. Foissy, "Potentiometric and conductometric analysis of the binding of Barium ions with alkali polyacrylate", *Colloid Polymer Sci.*, **276** [12] (1998) 1088–1097.
41. R.L. Penn, J.F. Banfield, "Morphology development and crystal growth in nanocrystalline aggregates under hydrothermal conditions: Insights from titania", *Geochimica et Cosmochimica Acta*, **63** [10] (1999) 1549–1557.
42. F.C. Meldrum, H. Colfen, "Controlling mineral morphologies and structures in biological and synthetic systems", *Chem. Rev.*, **108** [11] (2008) 4332–4432.
43. R. Bury, B. Desmazieres, C. Treiner, "Interactions between poly(vinylpyrrolidone) and ionic surfactants at various solid/water interfaces: A calorimetric investigation", *Colloids Surfaces A: Physicochem. Eng. Aspects*, **127** [1-3] (1997) 113–124.
44. H. Wang, X. Qiao, J. Chen, X. Wang, S. Ding, "Mechanisms of PVP in the preparation of silver nanoparticles", *Mater. Chem. Phys.*, **94** (2005) 449–453.
45. Y. Kobayashi, A. Kosuge, M. Konno, "Fabrication of high concentration barium titanate/polyvinylpyrrolidone nano-composite thin films and their dielectric properties", *Appl. Surface Sci.*, **255** [5] (2008) 2723–2729.
46. V.J. Sovilj, L.B. Petrovic, "Influence of hydroxypropylmethyl cellulose-sodium dodecylsulfate interaction on the solution conductivity and viscosity and emulsion stability", *Carbohydrate Polymers*, **64** [1] (2006) 41–49.
47. K.M. Hung, W.D. Yang, C.C. Huang, "Preparation of nanometer-sized barium titanate powders by a sol-precipitation process with surfactants", *J. Eur. Ceram. Soc.*, **23** [11] (2003) 1901–1910.
48. H.S. Isbell, *Carobohydrates in Solution*, American Chemical Society, Washington, 1973.
49. N. Jongen, P. Bowen, J. Lemaitre, J.C. Valmalette, H. Hofmann, "Precipitation of self-organized copper oxalate polycrystalline particles in the presence of hydroxypropylmethylcellulose (HPMC): Control of morphology", *J. Colloid Interface Sci.*, **226** [2] (2000) 189–198.
50. J. Zhao, Y.J. Li, Q.L. Kuang, G.X. Cheng, "Effects of hydroxypropylmethylcellulose macromolecules used as organic template on the crystallization of $CaCO_3$", *Colloid Polymer Sci.*, **284** [2] (2005) 175–182.
51. N. Sarkar, L.C. Walker, "Hydration dehydration properties of methylcellulose and hydroxypropylmethylcellulose", *Carbohydrate Polymers*, **27** [3] (1995) 177–185.
52. C.J. Brinker, G.W. Scherer, *Sol-Gel Sience*, Academic Press, San Diego (CA), 1990.
53. S.R. Dickinson, K.M. McGrath, "Aqueous precipitation of calcium carbonate modified by hydroxyl-containing compounds", *Cryst. Growth Des.*, **4** [6] (11-3-2004) 1411–1418.
54. I.V. Markov, *Crystal Growth for Beginners*, World Scientific Publishing Co. Pte. Ltd., 1995.